Establishing the fiber bridging law by an inverse analysis approach

Lin, Y. and Karadelis, J.N.

On Establishing the Fibre Bridging Law by an Inverse Analysis Approach

Yougui Lin
Department of Civil Engineering Architecture and Building, Faculty of Engineering and Computing, Coventry University, Coventry, W Midlands, CV1 5FB, UK
John N Karadelis*
Department of Civil Engineering Architecture and Building, Faculty of Engineering and Computing, Coventry University, Coventry, W Midlands, CV1 5FB, UK

ABSTRACT
A method for establishing the relationship between stress and crack face opening for steel fibre reinforced concrete (SFRC) beams under three-point loading was proposed using inverse analysis. The relationships were set up in two parts: Fracture mechanics theory was used before the hinge formation, followed by a classical mechanics of materials approach after the hinge was formed. This methodology did not incorporate any assumptions and was validated by the construction of experimental load versus crack-mouth-opening-displacement (CMOD) curves and by predicting the experimental load vs. CMOD relationship for independent flexural tests on beams of different sizes. The proposed method can simulate and predict the complete flexural performance of SFRC beams under three-point bending.
Key words: fibre, bridging-law, inverse-analysis, roller-compacted-concrete, fracture-mechanics, mechanics-of-materials

INTRODUCTION

The addition of fibres to concrete is intended mainly to improve the mixture's tensile strength, flexural strength and flexural toughness. It is well known that the mechanical performance of fibre-reinforced concrete (FRC) structures is strongly dependent on the mechanical interaction between matrix and fibres. For a given matrix, the fibre content, the fibre tensile strength and their geometric aspect ratio play a central role on the composite mechanical response. The main benefit gained by the addition of fibre is the improvement of the performance of FRC members after cracking. After cracking, fibres are stretched out in the cracked section, hence resisting the crack to open further. Therefore the relationship between the tensile stress developing in the fibre and the crack opening displacement should fully characterize the contribution made by the fibre-matrix interaction.

In simulating the cracking performance of concrete, cracks are traditionally treated by means of classical continuum or smear-crack approaches (Etse et al. 2012). In recent years, advanced numerical techniques with embedded discontinuities have been proposed to capture the cracking performance within the domain of fracture mechanics. For example, the elemental-finite element method (E-FEM) and the nodal finite element method (X-FEM) were developed to capture discontinuity paths (Oliver et al. 2006), while the element-free Galerkin method was proposed to capture arbitrary crack growth and growing crack problems (Belytschko et al. 1995) etc. The aforementioned numerical models cover mainly micro, meso and macro-scale approaches for FRC simulation. However, in the framework of structural scale models, interesting and practitioner-oriented proposals are founded in terms of cross-sectional based formulations (Olesen 2001; Burratti et al. 2011; Caggiano et al. 2012), which lie in the classical continuum models.

The simulation of load vs. CMOD of SFRC beams in flexure, lying in the cross-sectional based formulations, can be classified into two categories: One is based on the material mechanics method and the other on the fracture mechanics method. For the mechanics of materials approach, three assumptions are usually adopted (Maalej and Li 1994; Zhang and Stang 1998; Nour et al. 2011):

(a) Linear distribution of stress across the un-cracked section;
(b) Tensile stress at the crack tip, being equal to the tensile strength of the material;
(c) Hinge formation after cracking.

Based on these assumptions, the relationships of load-CMOD and load-deflection were established by applying a global equilibrium condition.

The fracture mechanics-based method was based on the crack propagation criterion described by eqn.(1) (Ballarini et al. 1984; Foote et al. 1986; Zhang and Li 2004). A crack initiates and extends when the total stress intensity factor is equal to the matrix material toughness.

$$\mathrm{K_a} - \mathrm{K_b} = \mathrm{K_{IC,M}} \qquad (1)$$

Where: K_a and K_b are the stress intensity factors (SIF) induced by applied load and fibre bridging traction, respectively; $K_{IC,M}$ is the fracture toughness of the matrix under mode-I loading.

The three assumptions adopted in the mechanics of materials based simulation are obviously debatable, for the following reasons:

(a) The crack tip behaves in a different way than a hinge before the crack reaches the top of the beam;

(b) The tensile stress vanishes when the crack reaches the top of the beam. In addition, the fracture mechanics-based method does not incorporate any assumptions, indicating that the latter can be more rigorous than the former.

The fracture mechanics-approach used to simulate the crack propagation has been studied since 1980's. Visalvanich and Naaman (1983) used the fracture energy concept to study the extension of cracks. Ballarini et al. (1984) and Foote et al. (1986) employed the stress intensity factor to study the crack growth length and fracture resistance of a SFRC beam. Jenq and Shah (1986) combined mechanics of materials and fracture mechanics to simulate crack propagation in a SFRC beam under the three-point bending regimes with the aid of several assumptions. Recently, Zhang and Li (2004) simulated the crack propagation of SFRC beams under three-point bending by employing fracture mechanics, based on the criterion of eqn.(1). However, the methods proposed by the aforementioned literature can only simulate the short load-CMOD curves (CMODs were usually smaller than 2mm) for the simple reason that fracture mechanics is no longer valid after the crack reached the top of beams.

Relationship between Fibre Tensile Stress and Crack Opening Displacement.

It seems that whatever the choice of the method, both methods resort to the same relationship of fibre tensile stress and crack opening displacement, usually named the Fibre Bridging Law, or $\sigma(w)$-w law for convenience (Lindhagen et al. 2000; Zhang and Li 2004). The fibre bridging law of SFRC has been investigated since the 1980's (Stroeven et al. 1978; Li and Wu 1992; Baggott and Abdel-monem 1992; Li and Chan 1994; Zhang and Stang 1998; Guo et al. 1999; Kazemi et al. 2007). Studies on $\sigma(w)$-w law can be categorized into two groups: Explicit consideration of fibre bridging mechanisms and non-explicit fibre contributions. The former resorts to pulling out individual fibres, or aligned fibres, to obtain a relationship of the tensile force, versus fibre slip. Fibre pull-out test, including normal fibre and inclined fibre pull-out, provides precise insight into the behaviour of the relationship of tensile stress and fibre slip displacement (Li and Chan 1994; Armelin and Banthia 1997; Laranjeira et al. 2010). However, the fibre bridging law cannot be obtained directly from these tests because fibres randomly distributed in the matrix behave differently to that in single fibre or aligned fibres tests. Several factors, such as the global orientation factor and the volumetric fraction of fibre, have to be taken into account in establishing the $\sigma(w)$-w law. Among these factors considered, the global orientation factor and effective volumetric fraction cannot be tested, and thus their values would be a guess (Foote et al. 1986, Jenq and Shah 1986). Therefore, it seems ideal to establish $\sigma(w)$-w laws by directly analysing load-CMOD or load-deflection using an inverse analysis approach, as it is often used to simulate the load-deformation response.

FIBRE BRIDGING LAW BY INVERSE ANALYSIS

It is certainly not viable to plant fibres in roller-compacted concrete (RCC) for pull-out tests. It is even more difficult to fabricate SFR-RCC (Steel Fibre Reinforced-Roller Compacted Concrete) dog-bone shape specimens for direct tensile tests and compact them with a vibrating compactor, due to mixes being very dry. Thus, the fibre bridging law for SFR-RCC may only be determined by an indirect method. The inverse analysis method, or back analysis technique, has been employed to establish the *σ(w)-w* law by the following researchers: Guo et al. (1999) proposed a method for determining *σ(w)-w* laws for the tail of load-deflection curve utilising mechanics of materials. Sousa and Gettu (2006) employed an analytical solution based on the hinge concept proposed by Stang and Oleson (1998, 2000) to establish *σ(w)-w* laws of concrete and SFRC. Slowik et al. (2006) developed explicit software for obtaining the *σ(w)-w* laws of concrete and SFRC from experimental results and employed the inverse analysis method. The latter enclosed an optimization procedure and a finite element analysis (FEA) programme. Kwon et al. (2008) also developed a FEA program calibrated with experimental results to obtain the *σ(w)-w* laws of concrete and SFRC. Recently Zhang and Ju (2011) derived *σ(w)-w* laws of SFRC by inverse analysis using the concept of cracking strength. All the above methods were based on the mechanics of materials approach. To the authors' best knowledge no researchers have established the *σ(w)-w* laws by employing both, an inverse analysis approach based on fracture mechanics and mechanics of materials theories yet.

The main objective of this article is to set-up a theoretical method for establishing the relationships between fibre tensile stress and crack face opening displacement, without introducing any assumptions. This method should be used to simulate and predict the flexural performance of SFRC beams from the beginning to the long tail-end of the crack history and therefore reveal the role of steel fibres as a means of reinforcement in concrete beams undergoing flexure. This method is established by employing fracture mechanics and material mechanics, respectively.

This article adopts the following procedure: First, it develops the SIFs (stress intensity factors) at crack tip and the relationships of load-CMOD (crack mouth opening displacement) induced by both, applied load and fibre tensile stress. The above is tracked by a mathematical technique for establishing the fibre bridging law by inverse analysis approach. The subsequent section describes the materials, specimen preparation and test procedure. The establishment of fibre bridging laws, using the proposed method is presented thereafter. The above is shadowed by three established fibre bridging laws, used to simulate the experimental load-CMOD curves to validate the bridging laws in a polynomial form. In the next section, an established bridging law in conjunction with the size effect law is employed to predict the load-CMOD curve for beams of different size. The prediction is compared with the experimental load-CMOD curves. Finally, the last section summarises all useful remarks and draws the appropriate conclusions

THE DEVELOPMENT OF LOAD v CMOD RELATIONSHIP

Crack Propagation of Notched Beam under Three-Point Bending (3PB) Test

Observations on SFRC beams under three-point bending tests indicated that all cracks initiated from the notch tip and extended monotonically with load increments. The cracks continued to extend although the applied load started falling after the peak load was reached and a hinge formed beneath the top of the beam. The hinge was located at about 0.1h beneath the top (h is the height of the beam). The complete process of failure of SFRC beam in flexure consisted of two distinct stages: The stage prior to hinge formation (Stage-I) and the stage after the hinge formation (Stage-II). In the former, the crack propagates monotonically and thus the process can be studied by fracture mechanics. In the latter the crack no longer extends and thus fracture mechanics is no longer valid and therefore mechanics of materials should take over. It is therefore apparent that two diverse relationships are needed to portray the stress vs. crack-face-opening-width.

The Form of σ(*w*)-*w* Law

Several forms of σ(*w*)-*w* laws, such as an exponential function proposed by Jenq and Shah (1986), and a complex expression by Armelin and Banthia (1997), have been used to simulate the load-CMOD path of SFRC beams in flexure. RILEM (2002) recommended four types of expressions, including multi-linear and bi-linear functions, to fit an experimental stress-crack opening curve from a uniaxial tension test, to obtain the σ(*w*)-*w* law for design purposes. Zhang and Stang (1998) conducted a direct tensile test of a notched SFRC bar and then established a *σ(w)-w* law using a regression fitting technique. This was a series of straight lines, representing the ascending and descending segments in the pre-peak and post-peak regions. The *multi-straight line bridging law* that was directly derived from a uniaxial test, was successfully used to simulate the load-CMOD relation of SFRC beams in flexure (Zhang and Li 2004). Therefore, a multi-linear function has been adopted to establish the σ(*w*)-*w* laws in later analysis.

Profile of Crack Face

Cox and Marshall (1991) proposed a self-consistency concept to analyse the crack face profile. Zhang and Li (2004) employed the concept to determine the crack profile for predicting load-CMOD curves of SFRC beams under 3PB test. However, the computation was a rather complicated and time-consuming iterative procedure. Fortunately, Foote et al. (1986) verified that the straight-line crack profile assumption was sufficiently accurate for calculating fracture parameters by comparing the exact and the approximate solutions. Since then, linear crack profiles have successfully been used in many studies (Jenq and Shah 1986; Maalej and Li 1994; Armelin and Banthia 1997; Zhang and Stang 1998; Song et al. 1999; Denneman et al. 2011; Nour et al. 2011). Therefore, the straight-line crack face assumption is employed in the analysis to follow.

Stress Intensity Factor and CMOD at Stage-I

At Stage-I the crack propagates monotonically, thus fracture mechanics can be applied. Consider the SFRC beam under three point bending (3PB) test shown in Figure 1, which shows the fibre tensile stress acting on the crack face. The total stress intensity factor (SIF) at the crack tip is the sum of that induced by the applied load P plus the fibre bridging stress, $\sigma(w(x))$. The crack initiates from the tip of the initial notch when the SIF is equal to the fracture toughness of matrix $K_{IC,M}$; and (the crack) continues advancing as the load increases. After the peak load is reached, the load decreases with crack growth in a displacement control mode. The criterion described by eqn.(1) is always satisfied during crack propagation in Stage-I.

Stress Intensity Factor and CMOD Induced by Applied Load.

Tada et al. (2000) provide the equations stated below for calculating SIF and CMOD of an unreinforced beam under 3PB induced by applied load:

$$K_{Ia} = \sigma\sqrt{\pi a}F\left(\frac{a}{h}\right) \tag{2}$$

$$CMOD_a = \frac{4\sigma a}{E} V\left(\frac{a}{h}\right) \tag{3}$$

$$\sigma = \frac{3PS}{2Bh^2} \tag{4}$$

$$F\left(\frac{a}{h}\right) = \frac{1.99 - \frac{a}{h}\left(1-\frac{a}{h}\right)\left(2.15 - 3.93\frac{a}{h} + 2.7\left(\frac{a}{h}\right)^2\right)}{\sqrt{\pi}\left(1+2\frac{a}{h}\right)\left(1-\frac{a}{h}\right)^{1.5}} \tag{5}$$

$$V = 0.76 - 2.28\left(\frac{a}{h}\right) + 3.87\left(\frac{a}{h}\right)^2 - 2.04\left(\frac{a}{h}\right)^3 + \frac{0.66}{\left(1-\frac{a}{h}\right)^2} \tag{6}$$

Where: K_{Ia} is the SIF induced by the applied load; $CMOD_a$ is the CMOD induced by the applied load; σ is the tensile stress evaluated by eqn. (4); P is the applied load; B, h, S and a are the width, height, span and length of crack; E is the Modulus of Elasticity of the material of the beam.

Stress Intensity Factor and CMOD Induced by Fibres

The relationships for evaluating SIF and CMOD induced by fibres are developed by the method of Green's function and Paris' Equation (Tada et al. 2000). The relationship for evaluating the SIF induced by fibres is:

$$K_{Ib} = \frac{2}{\sqrt{\pi a}} \int_{a_0}^{a} \frac{G\left(\frac{x}{a}, \frac{a}{h}\right) \sigma(w(x))}{\left(1-\frac{a}{h}\right)^{1.5} \sqrt{1-\left(\frac{x}{a}\right)^2}} dx \tag{7}$$

Where: K_{Ib} is the SIF induced by fibre traction; a_0 is the depth of the notch; x is defined in Figure1(b); $\sigma(\mathrm{w}(x))$ is the fibre bridging law; $G\left(\frac{x}{a},\frac{a}{h}\right)$ is Green's function evaluated by eqns. (8)-(12) below.

$$G\left(\frac{x}{a},\frac{a}{h}\right) = g_1\left(\frac{a}{h}\right) + g_2\left(\frac{a}{h}\right)\cdot\frac{x}{a} + g_3\left(\frac{a}{h}\right)\cdot\left(\frac{x}{a}\right)^2 + g_4\left(\frac{a}{h}\right)\cdot\left(\frac{x}{a}\right)^3 \tag{8}$$

$$\mathrm{g}_1\left(\frac{\mathrm{a}}{\mathrm{h}}\right) = 0.46 + 3.06\left(\frac{\mathrm{a}}{\mathrm{h}}\right) + 0.84\left(1-\frac{\mathrm{a}}{\mathrm{h}}\right)^5 + 0.66\left(\frac{a}{h}\right)^2\left(1-\frac{\mathrm{a}}{\mathrm{h}}\right)^2 \tag{9}$$

$$g_2\left(\frac{\mathrm{a}}{\mathrm{h}}\right) = -3.52\left(\frac{a}{h}\right)^2 \tag{10}$$

$$g_3\left(\frac{\mathrm{a}}{\mathrm{h}}\right) = 6.17 - 28.22\left(\frac{a}{h}\right) + 34.54\left(\frac{a}{h}\right)^2 - 14.39\left(\frac{a}{h}\right)^3 - \left(1-\frac{a}{h}\right)^{1.5} - 5.88\left(1-\frac{a}{h}\right)^5 -$$

$$-2.64\left(\frac{a}{h}\right)^2\left(1-\frac{a}{h}\right)^2 \tag{11}$$

$$g_4\left(\frac{\mathrm{a}}{\mathrm{h}}\right) = -6.63 + 25.16\left(\frac{\mathrm{a}}{\mathrm{h}}\right) - 31.04\left(\frac{a}{h}\right)^2 + 14.14\left(\frac{a}{h}\right)^3 + 2\left(1-\frac{a}{h}\right)^{1.5} + 5.04\left(1-\frac{a}{h}\right)^5 +$$

$$+1.98\left(\frac{a}{h}\right)^2\left(1-\frac{a}{h}\right)^2 \tag{12}$$

In order to apply Paris' Equation to obtain the CMOD induced by fibres, one has to exert a virtual pair of forces F acting at the crack mouth (see Figure1) (Tada et al. 2000). The stress intensity factor, K_{IF}, induced by the pair of these forces is then given by:

$$K_{IF} = \frac{2F}{\sqrt{\pi a}}\cdot\frac{G\left(\frac{0}{a},\frac{a}{h}\right)}{\left(1-\frac{a}{h}\right)^{1.5}\sqrt{1-\left(\frac{0}{a}\right)^2}} \tag{13}$$

Paris' Equation for plane stress conditions is (Tada et al. 2000):

$$CMOD = \frac{2}{E}\int_0^a K_{Ib}\,\frac{\partial K_{IF}}{\partial F}\,da \tag{14}$$

Applying Paris' Equation and replacing a in the integrand with a', to avoid confusion, results in:

$$CMOD_b = \frac{8}{\pi E}\int_0^{a}\left[\int_{a_0}^{a}\frac{G\left(\frac{x}{a'},\frac{a'}{h}\right)G\left(\frac{0}{a'},\frac{a'}{h}\right)}{\left(1-\frac{a'}{h}\right)^3\sqrt{1-\left(\frac{x}{a'}\right)^2}}\frac{\sigma(w(x))}{a'}dx\right]da' \qquad (15)$$

Where: $CMOD_b$ is the CMOD induced by fibre traction; *x* is as per Figure1(b).

For a relatively straight crack face, the crack opening displacement, *w*, at *x* is:

$$w = \frac{CTOD}{a-a_0}\cdot(a-x) \qquad (16)$$

Where: *w* is the crack opening displacement at *x*; *CTOD* is the notch tip opening displacement.

Therefore, for the SFRC beam the total CMOD is evaluated as follows:

$$CMOD = CMOD_a - CMOD_b \qquad (17)$$

Where: $CMOD_a$ and $CMOD_b$ are the CMODs induced by applied load and fibre tensile stress, respectively and evaluated by eqn.(3) and eqn.(15), respectively.

It is noted that in eqn.(15) the expression $1-\left(\frac{x}{a'}\right)^2$ may take a negative value due to the fact that variables a' and *x* are integrated over the intervals [0, a] and [a_0, a], resulting in *x* being larger than a', and consequently leading to the radical $\sqrt{1-\left(x/a'\right)^2}$ being a complex number. For engineering applications the applicable value for $CMOD_b$ is the real part of the complex quantity. This was discussed broadly by Xiao and Karihaloo (2002). The right hand side of eqn.(15) is singular at the lower bound integral for variable a'. Thus, Gaussian quadrature (Richard et al. 2005) was employed to avoid singularity problems and was achieved by numerical computation.

Development of Load-CMOD Relationship in Stage-II

After a hinge formation beneath the top of the beam, the concept of SIF at the crack tip is no longer valid. In fact, the criteria for crack extension defined by eqn.(1) would not be satisfied after the hinge formation. However, in this case the tensile stress on the crack face can be considered by using the mechanics of materials approach.

Observations during tests indicated that the hinge is usually formed at post-peak regions, when the load was decreasing as the CMOD was increasing. The SIF induced by fibre traction increases monotonically at stage-I, due to the increase of crack opening and propagation. However, the incremental rate of SIF induced by the applied load slows down due to the load reduction, although the crack length increases. When the criterion of eqn.(1) is not satisfied, this indicates a hinge formation.

Figure 2 shows a cut through the symmetry line of a SFRC beam under 3PB test, in which the crack reaches the top of the beam, and a hinge forms. The fibre tensile stress distributed on the crack face consists of $\sigma_I(w)$ and $\sigma_{II}(w)$. The bending moments caused by applied load and fibre tensile stress with respect to the hinge are:

$$M_P = \frac{PS}{4} \tag{18}$$

$$M_f = B\int_{a_0}^{h} \sigma(w(x))(h-x)dx \tag{19}$$

Where: M_P and M_f are the bending moments induced by applied load and fibre traction, respectively.

Application of global equilibrium condition with respect to the bending moments results in:

$$\frac{PS}{4} = B\int_{a_0}^{h} \sigma(w(x))(h-x)dx \tag{20}$$

Where: $\sigma(w(x))$ is the fibre bridging law, consisted of $\sigma_I(w) - w$ and $\sigma_{II}(w) - w$; Applying the assumption of straight crack face, the relations of CTOD and CMOD and crack width at x are:

$$w(x) = \frac{h-x}{h} \cdot CMOD \tag{21}$$

$$CTOD = \frac{h-a_0}{h} \cdot CMOD \tag{22}$$

Assuming that a hinge forms at $w = w_0$, the fracture mechanics-based method is valid in the interval [0, w_0]. Thus the corresponding length x_0 over which the bridging law, $\sigma_I(w) - w$, has been previously established, and is still valid is:

$$x_0 = \frac{w_0(h-a_0)}{CTOD} \tag{23}$$

The bending moment about the hinge induced by fibres is evaluated by:

$$M_f = B\int_{h-x_0}^{h} \sigma_I\big(w(x)\big)(h-x)dx + B\int_{a_0}^{h-x_0} \sigma_{II}\big(w(x)\big)(h-x)dx \tag{24}$$

Calculation Procedure

It has been previously stated that the real shape of fibre bridging law, established by Zhang and Stang (1998) using the results of the uniaxial tension test of SFRC bar, consists of a series of straight lines. Therefore, a linear function is used to establish the $\sigma(w) - w$ law by inverse analysis. Figure 3 shows the straight lines that constitute the bridging law. The calculation procedure is illustrated in Figure 4.

$$\left|(K_{Ia} - K_b - K_{IC,M})\right| \le \varepsilon_1 \tag{25}$$

$$|(CMOD - CMOD_i)| \le \varepsilon_2 \tag{26}$$

$$\left|(\frac{M_P - M_f}{M_P})\right| \le \varepsilon_3 \tag{27}$$

$$\sigma_i(w) = \sigma_i + \frac{\sigma_{i+1} - \sigma_i}{w_{i+1} - w_i}(w - w_i) \tag{28}$$

Where: ε_1, ε_2 and ε_3 are allowable tolerances; *CMOD* is the sum of calculated Crack-Mouth-Opening-Displacement shown in eqn.(17); Suffix *i* provides the experimental data (w_i, $\sigma(w)_i$) for *i*=1, 2, 3, ······(Figure 3).

During the iterative procedure, the crack length a_i should always be longer than the previous length a_{i-1}, in order to ensure a monotonically increasing crack length for the crack propagation in Stage-I. Considering the computation in stage-I, a_i and $\sigma(w)_i$ consist a solution when the criteria of eqns.(25) and (26) are satisfied for a given set of experimental data ($CMOD_i$, $CTOD_i$, P_i). On the other hand, in stage-II, $\sigma(w)_i$ is the solution when the criteria of eqns.(27) are satisfied for a set of data ($CTOD_i$, P_i).

EXPERIMENTAL CAMPAIGN AND RESULTS

Materials and Specimen Preparation

Mixes were purposely designed for concrete bonded overlay on old concrete pavements. They were named steel fibre-reinforced, roller-compacted SBR (Styrene Butadiene Rubber) modified concrete (SFR-RC-SBRMC). They were purposely designed to be placed by asphalt pavers and compacted by rollers. Five groups of beams made of five different mixes were prepared, containing the hooked-end steel fibre and the polymer SBR. Two types of steel fibre were used: one was 35mm long with aspect ratio 50, the other was 50mm long with aspect ratio 80. The mix design method, ingredients of the mixes, specimen formation and curing procedure can be found in Lin et al. (2013).

The specimens comprised centrally notched beams, tested under 3PB. The mix proportion is listed in Table 1, while the dimensions of the beams are reported in Table 2. Among the beams used, two beams of SBRPMC1.5%-35-L125 were purposely made for investigating the size effect on flexural strength. Mix SBRPMC1.5%-35 and SBRPMC1.5%-50 contained 35 mm-long and 50 mm-long fibres in the content of 1.5% by volume. SBRPMC0% acted as the matrix of the mixes. All three mixes were the same, only mix SBRPMC0% did not contain any fibres. The beams were compacted with a vibrating compactor, specially designed for the present research study.

Mix Con.SBRPMC1.5%-35 was conventional concrete, containing the same steel fibres as mix SBRPMC1.5%-35. Its fresh mix exhibited a slump of 130mm. Con.SBRPMC0% was the matrix of Con.SBRPMC1.5%-35; the mix proportion of both mixes was the same except that the matrix did not contain fibres. Beams of the two mixes were purposely employed to reveal the fibre efficiency in both, conventional concrete and roller-compacted concrete, by comparing the fibre bridging laws of the two mixes. The mix was casted in steel moulds and consolidated on the vibrating table.

The beams of matrixes SBRPMC0%-L67 and Con.SBRPMC0%-L67 were saw-cut at mid-span to a 33mm deep notch to comply with the RILEM code (1991). At this point it seems opportune to provide more explanation for the identification number of the beams. Considering mix Con.SBRPMC1.5%-35-L80 as an example, this indicates that the mix is conventional SBR polymer modified concrete, containing 1.5% 35mm-length fibre in volume fraction, whereas the ligament height is 80mm.

Tests of Matrix Beams

The experimental setup for measuring fracture toughness in Mode-I loading is shown in Figure 5. The test machine comprised a hydraulic servo-closed loop with a maximum load capacity of 150 KN. Test data were automatically recorded by a computer at the frequency of 5 Hz. The span-to-depth ratio and notch-length to depth ratio were 4 and 0.33, respectively. The test procedure complied with the RILEM code (1991). However, the loading rate and the unloading procedure recommended by RILEM were not followed. The load was controlled by CMOD at the incremental rate of 0.0001 mm/s, significantly lower than that recommended by RILEM. It was, however, consistent in all flexural tests. CMOD, CTOD and load-point deflection were measured and recorded automatically by a computer during the test. The measurement of CTOD at maximum load was taken as the critical crack tip opening displacement ($CTOD_C$). The Two-parameter model proposed by Jenq and Shah (1985) and adopted by the RILEM (1991) was employed. The critical stress intensity factor ($K_{IC,M}$), was determined based on the RILEM code. In the meantime, the stress intensity factor corresponding to crack initiation at the notch tip ($K_{IC,M}^{ini}$), modulus of rupture (MOR) and compressive strength (f_c) were determined from the same test data and listed in the same Table 3. The method to determine $K_{IC,M}^{ini}$ was the same as that proposed in Double-K model by Xu and Reinhardt (1999). The load corresponding to crack initiation at notch tip was obtained by identifying the change of load-CMOD curve from linear to non-linear.

Test Procedure of SFR-RC-SBRMC Beams

The experimental setup for testing notched SFR-RC-SBRMC beams under 3PB is the same as the one used in matrix beams, shown in Figure 5. Load, CMOD, CTOD and vertical displacement at mid-span were measured, and the test data were automatically recorded by a computer at the frequency of 5 Hz. The loading rate was controlled by CMOD, such as: 0.0001 mm/s up until CMOD was equal to 0.2 mm; then 0.0033 mm/s up until CMOD was equal to 3 mm; then 0.005 mm/s until complete failure of the specimen occurred. The experimental results used to establish the fibre bridging laws are presented in the succeeding sections.

Mechanical Properties of Mixes

Table 3 shows the mechanical properties of mixes SBRPMC1.5%-35, SBRPMC1.5%-50 and Con.SBRPMC1.5%-35. The compressive strength, f_c, was measured by using blocks sawn off the tested beams. The MOR (modulus of rupture) was evaluated using the maximum load and the geometrical dimension of the notched cross-section of the beam. The Moduli of Elasticity and Poisson's ratios of mixes SBRPMC1.5%-35 and Con.SBRPMC1.5%-35 listed in Table 3 were measured using cylinders of Φ100mm x H180mm in compression. The Modulus of Elasticity and Poisson's ratio of mix SBRPMC1.5%-50 was simply taken as that of mix SBRPMC1.5%-35, since both mixes were the same except for the fibre length.

Establishing the Bridging Law for SFR-RC-SBRMC

The calculation procedure has been presented earlier. MatLab was utilised for the computations (Valentine and Hanhn 2007). 6 x 6 Gaussian integrating points (Richard et al. 2005) were used to perform the double-variable integration for $CMOD_b$ and six Gaussian integrating points were used for K_{Ib} and M_f. The allowable tolerance of ε_1 was usually taken to be within the range of 2-6 MPa·mm$^{0.5}$, that of ε_2 was in the range of 0.008-0.02 mm and that of ε_3 was less than 0.01. The variable allowable tolerance for ε_1 and ε_2 was chosen to achieve computational convergence and a unique solution. Calculations showed a hinge forming at the crack length, *a*, being approximately equal to 0.9h. This is consistent with the observation results during the test, which have been declared previously.

In order to demonstrate the method proposed earlier, the SBRPMC1.5%-35-L80 beam with 20mm notch depth, under 3PB is taken as a case-study to establish the fibre bridging law. The experimental load-CMOD curves of the four beams are plotted in Figure 10(a) and the averages of CMOD, CTOD and P of the four beams at specific CMOD values are listed in Table 4. It is noted that the load P, in Table 4, is the applied load for 1 mm width of beam. The calculated $\sigma(w)$ and the corresponding *w* are tabulated in Table 4 too. The fracture mechanics-based method was applicable until the crack face opening was equal to 0.958mm

($w_0 = 0.958\ mm$). Afterwards, a hinge formed beneath the point load and the mechanics of materials theory was utilised. The displacement range in Stage-I was 0.121 – 0.958 mm, while that in Stage-II was in the range of 0.958 – 12.45 mm. The established fibre bridging law for mix SBRPMC1.5%-35 is plotted in Figures 6 & 7.

Figures 6 and 7 show clearly that the profile of the established *σ(w)-w* relationship using inverse analysis, is quite similar to the experimental one under direct tensile tests, as illustrated in the literature by Zhang and Stang (1998). This validates the method for establishing *σ(w)-w* as proposed earlier. The regression fitted polynomial for the calculated stress *σ(w)* and crack face opening *w* represents its general tendency.

The procedure for establishing the fibre bridging law for the other two mixes Con.SBRPMC1.5%-35 and SBRPMC1.5%-50 is similar. The results are illustrated in Figures 8 and 9. The fitted polynomials for the fibre bridging laws are shown in the same figures and listed in Table 5.

Simulating Load-CMOD

It has been previously pointed out that the bridging law, as defined by a polynomial, represents approximately only the general tendency of the experimental load-CMOD. Therefore, it may be appropriate to back the polynomial bridging law by validating the load-CMOD relationship. The fibre bridging law established previously and listed in Table 5 is used to simulate the relationship of load-CMOD at crack initiation (the notch tip), in Stage-I, and in Stage-II.

Load and CMOD during Crack Initiation at Notch Tip

Before cracking of the matrix takes place the fibres are inactive, thus the very first crack birth is resisted by the matrix only. The load causing crack initiation at notch tip can be evaluated using eqn.(2) by setting $a=a_0$ and $K_{Ia} = K_{IC,M}^{ini}$. The CMOD is calculated using eqn.(3) with a known load. The critical stress intensity factor of the matrix for crack initiation at notch tip is listed in Table 3.

Simulating Stage-I

In stage-I, in which the notch tip opening displacement (CTOD) is less than w_0, the fracture mechanics method is used. The establishment of the load-CMOD relationship takes place by calculating the load *P* for a given *CMOD*. Thus, for a given *CMOD*, vary *P* and crack length *a*, and then calculate K_{Ia}, K_{Ib}, $CMOD_a$ and $CMOD_b$. *P* and *a* are the solutions when the criteria of eqns. (25) & (26) are satisfied. Assuming a straight crack face, the CTOD is calculated by:

$$CTOD = \frac{a-a_0}{a} \cdot CMOD \tag{29}$$

Simulating Stage-II

In Stage-II, in which the notch tip opening displacement (CTOD) is larger than w_0, the Mechanics of Materials method is used. The establishment of the load-CMOD relationship can be achieved by calculating the load *P* for a given *CMOD*. Thus for a given *CMOD*, vary

P and then calculate x_0 and M_P and M_f. When the criterion of eqn.(27) is satisfied, the corresponding value of P represents the solution.

Discussion

The results from the numerical simulation are plotted and compared with the experimental results in Figures 10 and 11. It is reminded that the load shown in both figures is the applied load for 1mm width of beam. Also, it is pointed out that the clip gauges for measuring CMOD of Beams 3 and 4, made of mix SBRPMC1.5%-35, disengaged abruptly during the test, at CMOD=3.6mm for Beam-3 and 10.2mm for Beam-4, as shown in Figure 10(a). It should also be mentioned that three beams of mix SBRPMC1.5%-50-L80 were prepared. Two beams were centrally saw-cut to a notch depth of 19mm. Unfortunately, the third beam was notched 25mm (target depth was 20mm). The experimental load-CMOD curve of the third beam was far below the curves of the other two beams. Thus, its experimental data are not used and its curve is not presented in Figure 11. It is accepted that the transition from fracture mechanics to mechanics of materials approach is visible at the simulation curves plotted in Figures 10(a) and 11. However, the differences at the transition points are fairly small from the viewpoint of engineering applications.

It is apparent that the simulated load-CMOD curves are in good agreement with the experimental results. It is also clear that with the aid of the established bridging law, the proposed method can simulate the flexural performance of SFRC beams from the origin to the long tail-end.

Prediction of Load-CMOD Relationship

In this study two beams of the mix SBRPMC1.5%-35 with the dimensions 100 mm x 150 mm x 500 mm width, height and span were tested, following the same procedure as in the beams of the same mix described previously. These beams were larger in size than the beams used for establishing the fibre bridging law listed in Table 5.in Table 5.

The relation of load-CMOD of the larger beams is predicted using the fibre bridging law, the calculation procedure proposed earlier and the size effect law. Research conducted by the authors (Lin 2014) indicated that the flexural strengths were significantly affected by the size of specimens. It was noted that the trajectories of the flexural strength-CMOD curves of the mix SBRPMC1.5%-35 beams with different ligament heights were nearly parallel to each other, especially in the post-peak region, indicating that the $\sigma(w) - w$ laws for different specimen size may be related by a constant factor.

Using mix SBRPMC1.5%-35, Lin (2014) confirmed experimentally the size effect law, in its form of Bazant’s Equation (Bazant 1989), by testing a total of eleven notched beams with ligament heights in the range of 40 – 125 mm. Essentially, he casted nine 80x100x400 mm beams, four of which had a 20 mm notch saw-cut at mid-span, three a 40 mm notch and two a 60 mm notch. The remaining two beams were made of 100x150x500 mm and were centrally notched 25 mm deep. The size effect equation for the mix SBRPMC1.5%-35 is:

$$f_p = \frac{80.42}{\sqrt{\frac{\mathrm{D}}{2.7} - 1}} \tag{30}$$

Where: f_p is maximum flexural strength (MPa); D is the height (depth) of ligament (mm).

The ligament height of the beam used for establishing the bridging law was 77.3mm (Table 4), whereas the average height of ligaments of the beams used for prediction is 123mm. Thus, the ratio of maximum flexural strength of the 123mm - ligament beam to that of the 77.3mm-ligament beam is 0.787, which is determined using eqn. (30). Therefore, the bridging law for the beam with the 123mm-height ligament is then:

$$\sigma(w) = 0.787 \times [-59.768w^5 + 146.64w^4 - 122.85w^3 + 37.82w^2 - 2.7337w + 5.193]$$

$$0 \leq w \leq 0.958 \text{ mm} \tag{31}$$

$$\sigma(w) = 0.787 \times [-0.0056w^3 + 0.1612w^2 - 1.5044w + 5.9306]$$

$$0.958 \leq w \leq 12.45 \text{ mm} \tag{32}$$

The procedure for the prediction of load-CMOD relationship is the same as that described previously. The prediction of load-CMOD using the bridging law above, is illustrated and compared with the experimental load-CMOD curves in Figure 12. It is noted that the clip gauge of beam-2 disengaged abruptly during the test at CMOD= 4 mm, hence a comprehensive experimental load-CMOD history is not available. It is observed that the predicted results are in good agreement with the experimental results as the maximum predicted load is only 8% higher than the measured one. It is obvious that the proposed method, combined with the established bridging law and size effect law, can predict the flexural performance of SFRC beams from the origin to the long tail-end.

REMARKS AND CONCLUSIONS

Summarizing the above, the following conclusions can be drawn:

An assumptions free method for establishing the performance of SFRC in flexure using an inverse analysis approach has been proposed. It has been proved experimentally and verified by simulating and predicting the load-CMOD relations of beams. The proposed method consists of two stages: Stage-I is defined as the stage before a hinge forms at the top of the beam. In this case the fibre bridging law was set up by using fracture mechanics. Stage-II defines the mechanics after the formation of a hinge. In this case the fibre bridging law was established by using mechanics of materials.

The established relationship between stress and crack face width can be regarded as the real stress distribution on the crack’s face. The general tendency of the established bridging laws for the mixes used in the study (Figures 10-12) is similar to that obtained by a direct tension test conducted by Zhang and Stang (1998).

The fibre bridging law is affected by specimen size. The combination of fibre bridging law and size effect law may be regarded as a material property. The method, combined with the established bridging law and size effect law, can predict the flexural performance of SFRC beams from the origin to the long tail-end.

Although the specimens used in the study were steel fibre-reinforced roller compacted SBR modified concrete, the proposed method for establishing the fibre bridging law can be suitable to any fibre reinforced concrete and even plain concrete.

Acknowledgements

The financial support of the Engineering and Physical Sciences Research Council (EPSRC Ind. Case Studentship, No. 08002550) and Aggregate Industries, UK, is gratefully acknowledged. The authors would like to express their gratitude to Ms. Yi Xu for her help in laboratory work, to the reviewers for their valuable comments, and also to Mr. Ian Breakwell, senior technician at the Civil Engineering Laboratories of Coventry University for his valuable suggestions, comments and help. Special mention should also be made to Tarmac, AGS Mineraux, Power Minerals and Nippon Gohsei EU for providing various materials for research.

References

Armelin, H.S.; Banthia, N.; 1997, Predicting the flexural post-cracking performance of steel fibre reinforced concrete from the pull-out of single fibres, ACI Materials Journal, V.94, No.1, January- February, 1997, 18-31.

Baggott, R.; Abdel-monem, A.E.S.; 1992, Aspects of bond in high volume fraction steel fibre reinforced calcium silicates, High Performance Fibre Reinforced Cement Composites, 15th Proceedings of RILEM and ACI workshop, Edited by H.W. Reinhard and A.E. Naanman.

Ballarini, R.; Shah, S.P., Keer, L.M.; 1984, Crack growth in cement-based composites, Engineering Fracture Mechanics, Vol.20, No.3, 433-445.

Bazant, Z.P.; 1989, Fracture energy of heterogeneous materials and similitude, in Fracture of Concrete and Rock, edited by Shah, S.P., and Swartz, S.E., Pringer-Verlag, New York, 1989, 229-241.

Belytschko, T.; Lu, Y.; Gu, L.; 1995, Crack propagation by element-free Galerkin methods, Engineering Fracture Mechanics, 51(2): 295-315.

Buratti, N.; Mazzotti, C.; Savoia, M.; 2011, Post-cracking behaviour of steel and macro-synthetic fibre-reinforced concrete, Construction and Building Materials, 25(5): 2713-2722.

Caggiano, A.; Cremona, M., Faella, C.; Lima, C.; Martinelli, E.; 2012, Fracture behaviour of concrete beams reinforced with mixed long/short steel fibres, Construction and Building Materials, 37:832-840.

Cox, B.N., Marshall, D.B.; 1991, Stable and unstable solutions for bridged cracks in various specimens, Acta, Metallic materials, Vol.39, No.4, 579-589.

Denneman, E., Wu, R., Kearsley, E.P., Visser, A.T.; 2011, Discrete fracture in high performance fibre reinforced concrete materials, Engineering Fracture Mechanics, 78 (2011), 2235-2245.

Etse, G., Caggiano, A., Vrech, S.; 2012; Multiscale failure analysis of fibre reinforced concrete based on a discrete model, International Journal of Fracture, 178: 131-146.

Foote, R.M.L., Mai, Y.W., Cotterell, B.; 1986, Crack growth resistance curves in strain-softening materials, Journal of Mechanics and Physics of Solids, Vol. 34, No.6, 593-607.

Guo, X.H., Tin-Loi, F., Li, H.; 1999, Determination of quasi-brittle fracture law for cohesive models, Cement and Concrete Research, 29 (1999), 1055-1059.

Jenq, Y.S.; Shah, S. P.; 1985, Two-parameter fracture model for concrete, Journal of Engineering Mechanics, Vol.111, No.10, 1227-1241.

Jenq, Y.S., Shah, S. P.; 1986, Crack propagation in fibre-reinforced concrete, Journal of Structural Engineering, 1986, Vol.112, No.1, 19-34.

Kazemi, M.T., Fazilah, F., Ebrahiminezhand, M.A.; 2007, Cohesive crack model and fracture energy of steel-fibre-reinforced-concrete notched cylindrical specimens, Journal of Materials in Civil Engineering, Vol. 19, No. 10, 884- 890.

Kwon, S.H.; Zhao, Z. Shah, S.P.; 2008, Effect of specimen size on fracture energy and softening curve of concrete: Part II. Inverse analysis and softening curve, Cement and Concrete Research 38 (2008), 1061–1069.

Laranjeira, F., Molins, C., Aguado, A., 2010, Predicting the pull-out response of inclined hooked steel fibres, Cement and Concrete Research, 40 (2010), 1471-1487.

Li, V.C., Wu, H.-C.; 1992, Pseudo strain-hardening design in cementitious composites, High Performance Fibre Reinforced Cement Composites, 15th Proceedings of RILEM and ACI workshop, Edited by H.W. Reinhard and A.E. Naanman.

Li, V.C., Chan, Y.M.; 1994, Determination of interfacial debond mode for fibre-reinforced cementitious composites, Journal of Engineering Mechanics, Vol.120, No.4, 707-719.

Lin, Y., Karadelis, J.N., Xu, Y.; 2013, A new mix design method for steel fibre-reinforced, roller compacted and polymer modified bonded concrete overlays, Construction and Building Materials 48 (2013), 333–341.

Lin, Y.; 2014, Optimum Design for Sustainable, 'Green' Bonded Concrete Overlays: Controlling Flexural Failure. PhD Thesis, Department of Civil Engineering, Architecture and Building, Faculty of Engineering and Computing, Coventry University, UK, (unpublished).

Lindhagen, J.E., Gamstedt, E.K, Berglund L.A.; 2000, Application of bridging-law concepts to short-fibre composites Part 3: Bridging law derivation from experimental crack profiles, Composites Science and Technology 60, 2883-2894.

Maalej, M., Li, V.C.; 1994, Flexural strength of fibre cementitious composites, Journal of Materials in Civil Engineering, Vol. 6, No. 3, 390-406.

Nour, A., Massicotte, B., Montaignac, R.D., Charron, J.P.; 2011, Derivation of a crack opening deflection relationship for fibre reinforced concrete panels using a stochastic model: Application for predicting the flexural behaviour of round panels using stress crack opening diagrams, Cement and Concrete Research, 41 (2011), 964-974.

Olesen, J.F.; 2001; Fictitious crack propagation in Fibre-reinforced concrete beams, Journal of Engineering Mechanics, 127(3):272-280.

Oliver, J., Huespe, A.E., Sanchez, P.J.; 2006, A comparative study on finite elements for capturing strong discontinuities: E-FEM vs X-FEM, Computer Methods in Applied Mechanics and Engineering, 195: 4732-4752.

Richard L., Burden, J., Douglas F, 2005, Numerical Analysis, 8th edition, Thomson Brooks/Cole.

RILEM, 1991, Fracture mechanics test method for concrete, Report 5, Edited by Shah, S.P. and Carpinteri, A.

RILEM TC 162-TDF, 2002, Test and design methods for steel fibre reinforced concrete. -Design of steel fibre reinforced concrete using σ–w method: Principles and applications, Chairlady: Vandewalle L, Materials and Structures, 35(2002), 262-278.

Slowik, V., Villmann, B., Bretschneider, N., Villmann, T.; 2006, Computational aspects of inverse analyses for determining softening curves of concrete, Computer Methods in Applied Mechanics and Engineering, 195 (2006), 7223–7236.

Song, G.M., Zhou, Y., Sun. Y.; 1999, Modelling of fibre toughening in fibre-reinforced ceramic composites, Ceramics International, (25) (1999), 257-260.

Sousa, J.L.A.O., Gettu, R.; 2006, Determining the tensile stress-crack opening curve of concrete by inverse analysis, Journal of Engineering Mechanics, Vol. 132, No. 2, 141–148.

Stang, H., Oleson, J.F.; 1998, On the interpretation of bending test on FRC materials, Proceedings, FRAMCOS-3, Fracture Mechanics of Concrete Structures, H. Mihashi and K. Rokugo, eds. Vol. I, Aedificatio Publisher, Freiburg, Germany, 511-520.

Stang, H., Oleson, J.F.; 2000, A fracture mechanics based design approach to FRC, Proceedings, 5th RILEM Symposium on Fibre-reinforced Concretes (FRCs), BEFIB 2000.

Stroeven, P., Shah, S.P., deHaan, Y.M., and Bouter, C.; 1978, Pull-out tests of steel fibres, Proceedings, International Symposium, RILEM-ACI-ASTM, Sheffield, England, 345-353.

Tada, H., Paris, P.C., Irwin, G.R.; 2000, The stress analysis of cracks handbook, (third edition), Professional Engineering Publishing.

Valentine, D.T., Hanhn, B.D.; 2007, Essential MATLAB for engineers and scientists (Electronic book), 3th edition.

Visalvanich, K., Naaman, A.; 1983, Fracture model for fibre reinforced concrete, ACI Materials Journal, March-April 1983, 128-138.

Xiao, Q.Z., Karihaloo, B.L.; 2002, A Proximate Green's functions for singular and higher order terms of an edge crack in a finite plate, Engineering Fracture Mechanics, 69 (2002), 959-981.

Xu, S., Reinhardt, H.W.; 1999, Determination of double-K criterion for crack propagation in quasi-brittle fracture, Part II: Analysis evaluating and practical measuring methods for three-point bending notched beams, International Journal of Fracture, 98 (1999), 151-177.

Zhang, J., Stang, H.; 1998, Applications of stress crack width relationship in predicting the flexural behaviour of fibre-reinforced concrete, Cement and Concrete Research, Vol. 28, No. 3, 439-452.

Zhang, J., Li, V.C.; 2004, Simulation of crack propagation in fibre-reinforced concrete by fracture mechanics, Cement and Concrete Research, 34 (2004), 333-339.

Zhang, J., Ju, X.; 2011, Investigation on stress-crack opening relationship of engineering cementitious composites using inverse approach, Cement and Concrete Research, 41 (2011), 903-912.

List of Figure Captions

Figure 1. (a) SFRC beam under three-point bending. (b) Fibre tensile stress distribution on crack faces.

Figure 2. A crack reaching the top of SFRC beam under three-point bending.

Figure 3. $\sigma(w) - w$ law consisting of multi-linear lines

Figure 4. Synoptic calculation procedure for establishing the fibre bridging law. Stage-I (left): Fracture Mechanics Method. Stage-II (right): Mechanics of Materials Method.

Figure 5 (a). Loading configuration and instrumentation. (b) Notched beam under three-point bending. The clip gauge for measuring CMOD, a LVDT for measuring CTOD, and a second LVDT for measuring load-point deflection are visible.

Figure 6. Calculated tensile stress $\sigma(w)$ for a given crack face opening w and regression fitting expressions for the SBRPMC1.5%-35-L80 beams under 3PB by inverse analysis (w_0= 0.958mm)

Figure 7. Calculated $\sigma(w)$-w for the SBRPMC1.5%-35-L80 beams under 3PB by inverse analysis using fracture mechanics, for w < 0.958mm

Figure 8. Calculated $\sigma(w)$ and w, and regression fitting expressions for the Con.SBRPMC1.5%-35-L80 beams under 3PB by inverse analysis (w_0= 0.907mm)

Figure 9. Calculated $\sigma(w)$ and w and regression fitting expressions for the SBRPMC1.5%-50-L80 beams under 3PB by inverse analysis (w_0=1.063mm).

Figure 10. Comparison between experimental load-CMOD curves with simulated curve: (a) mix SBRPMC1.5%-35, (b) mix Con.SBRPMC1.5%-35

Figure 11. Comparison of experimental load-CMOD curves with simulated curve of mix SBRPMC1.5%-50

Figure 12. Comparison of experimental load-CMOD curves with predicted curve of SBRPMC1.5%-35-L123beam

List of Tables with their Headings

Table 1
Mix proportion of the five mixes.

Mix ID	Mix proportion						Mix wet
	Cem.	Coarse aggre.	sand	SBR	added water	Fibre by volume	density (MPa)
SBRPMC1.5%-35	1	1.266	1.266	0.217	0.095	1.50%	2482
SBRPMC1.5%-50	1	1.266	1.266	0.217	0.095	1.50%	2480
Con.SBRPMC1.5%-35	1	1.266	1.266	0.217	0.244	1.50%	2330
SBRPMC0%	1	1.266	1.266	0.217	0.095	0%	2306
Con.SBRPMC0%	1	1.266	1.266	0.217	0.244	0%	2297

Table 2
Mixes and dimensions of tested beams for establishing the $\sigma - w$ laws by inverse analysis.

ID of beams	Num.of beams	Fibr. leng. mm	Dimen.of beam (mm) width x height x span	Ligament/notch (mm)
SBRPMC1.5%-35-L80	4	35	80x100x400	80/20
SBRPMC1.5%-35-L125	2	35	100x150x500	125/25
SBRPMC1.5%-50-L80	3	50	80x100x400	80/20
Con.SBRPMC1.5%-35-L80	2	35	100x100x400	80/20
SBRPMC0% -L67	3	-	80x100x400	67/33
Con.SBRPMC0%-L67	3	-	100x100x400	67/33

Table 3

Mechanical properties of mixes and their matrix

Mix ID	$K_{IC,M}$ (MPamm$^{0.5}$)	$CTOD_C$ (mm)	$K_{IC}^{ini}{}_{,M}$ (MPamm$^{0.5}$)	E (MPa)	ν	MOR(3PB) (MPa)	f_c (MPa)
SBRPMC1.5%-35				32365	0.187	15.22	79.61
SBRPMC1.5%-50				32365	0.187	16.76	
Con.SBRPMC1.5%-35				31000	0.19	10.37	68.18
SBRPMC0%	48.76	0.0104	24.63			7.93	75.5
Con.SBRPMC0%	41.36	0.0182	15.2			6.52	65.9

Table 4
Experimental data of beams SBRPMC1.5%-35-L80 under 3PB and calculated σ(w) for a given w by inverse analysis (P= applied load per 1mm width; dimensions: $h_{(ave)}$= 99.3mm, $a_{0(ave)}$= 22mm)

Type of theory	Average of experimental results			Calculated values for σ(w)-w	
	CMOD mm	CTOD mm	P N/mm width	w mm	σ(w) MPa
Fracture mechanics	0	0	0	0.000	5.2
	0.2	0.1206	137.4	0.121	5.2
	0.4	0.2495	147.6	0.250	5.5
	0.6	0.3676	154.6	0.368	5.5
	0.8	0.522	153.5	0.522	5.12
	1	0.663	151.8	0.663	4.93
	1.4	0.958	147	0.958	4.56
Mechanics of Materials	1.6	1.103	146.7	1.103	4.54
	2	1.407	138.4	1.407	4.22
	4	2.945	105.7	2.945	2.5
	6	4.497	82.7	4.497	1.94
	8	6.078	70.2	6.078	1.84
	10	7.646	60.2	7.646	1.06
	12	9.34	54.1	9.340	1.42
	14	10.9	50.5	10.900	1.42
	16	12.45	47.8	12.450	1.38

Table 5

Fibre bridging laws of mixes SBRPMC1.5%-35, Con.SBRPMC1.5%-35 and SBRPMC1.5%-50, as established for beams under 3PB.

Mix ID	Bridging law in flexure	
SBRPMC1.5%-35	$\sigma(w) = -59.768w^5 + 146.64w^4 - 122.85w^3 + 37.82w^2 - 2.7337w + 5.193$	$0 \le w \le 0.958$mm
	$\sigma(w) = -0.0056w^3 + 0.1612w^2 - 1.5044w + 5.9306$	0.958mm$\le w \le 12.45$mm
Con.SBRPMC1.5%-35	$\sigma(w) = -24.88w^3 + 26.568w^2 - 5.5956w + 3.3125$	$0 \le w \le 0.907$mm
	$\sigma(w) = 0.0012w^3 - 0.025w^2 - 0.0461w + 2.4392$	0.907mm$\le w \le 12.64$mm
SBRPMC1.5%-50	$\sigma(w) = 11.165w^3 - 22.287w^2 + 11.068w + 4.5571$	$0 \le w \le 1.063$mm
	$\sigma(w) = -0.0012w^3 + 0.0654w^2 - 0.9482w + 5.9164$	1.063mm$\le w \le 12.99$mm

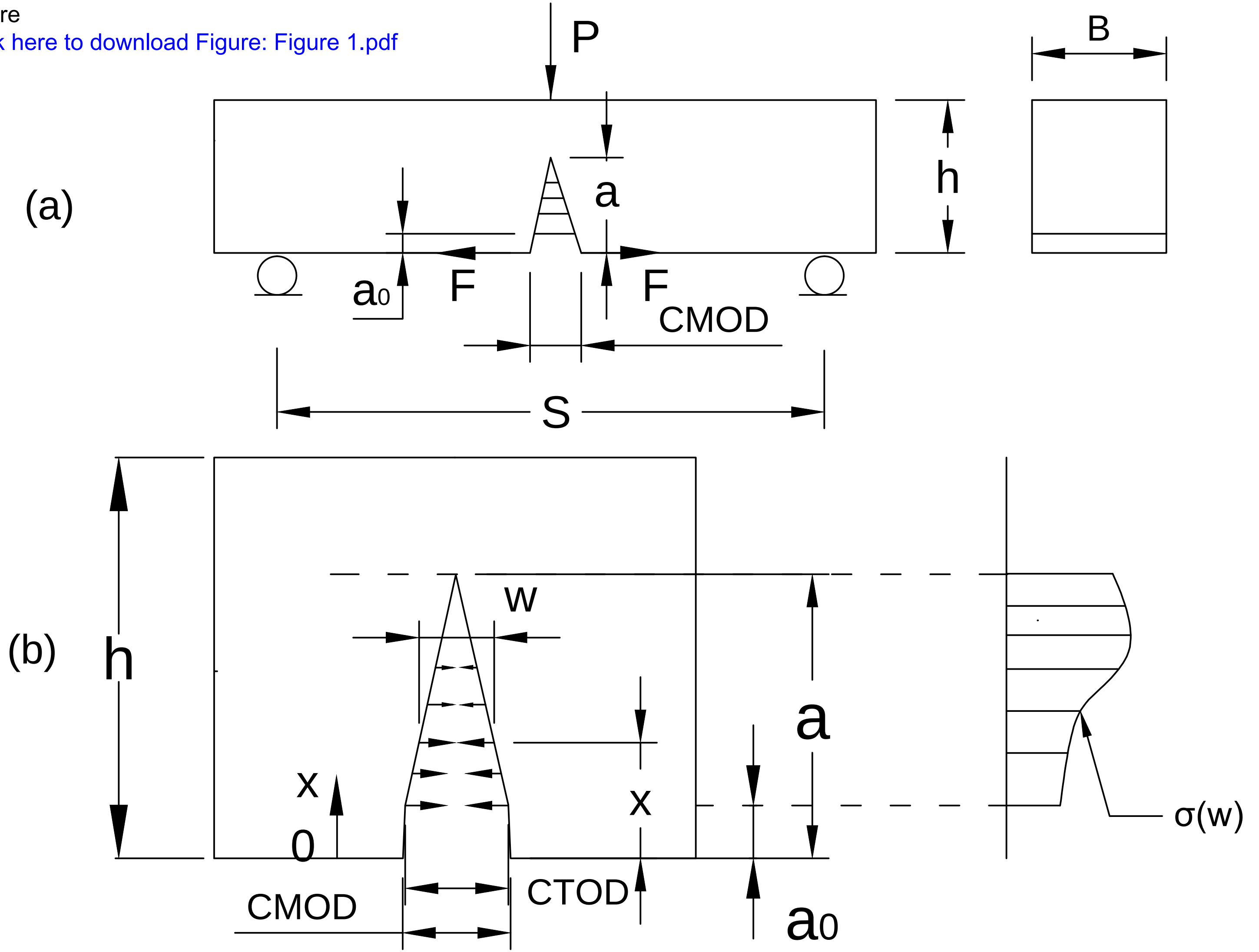
P
B
a
h
(a)
a0
F
F
CMOD
S
(b)
h
w
a
x
x
0
σ(w)
CMOD
CTOD
a0

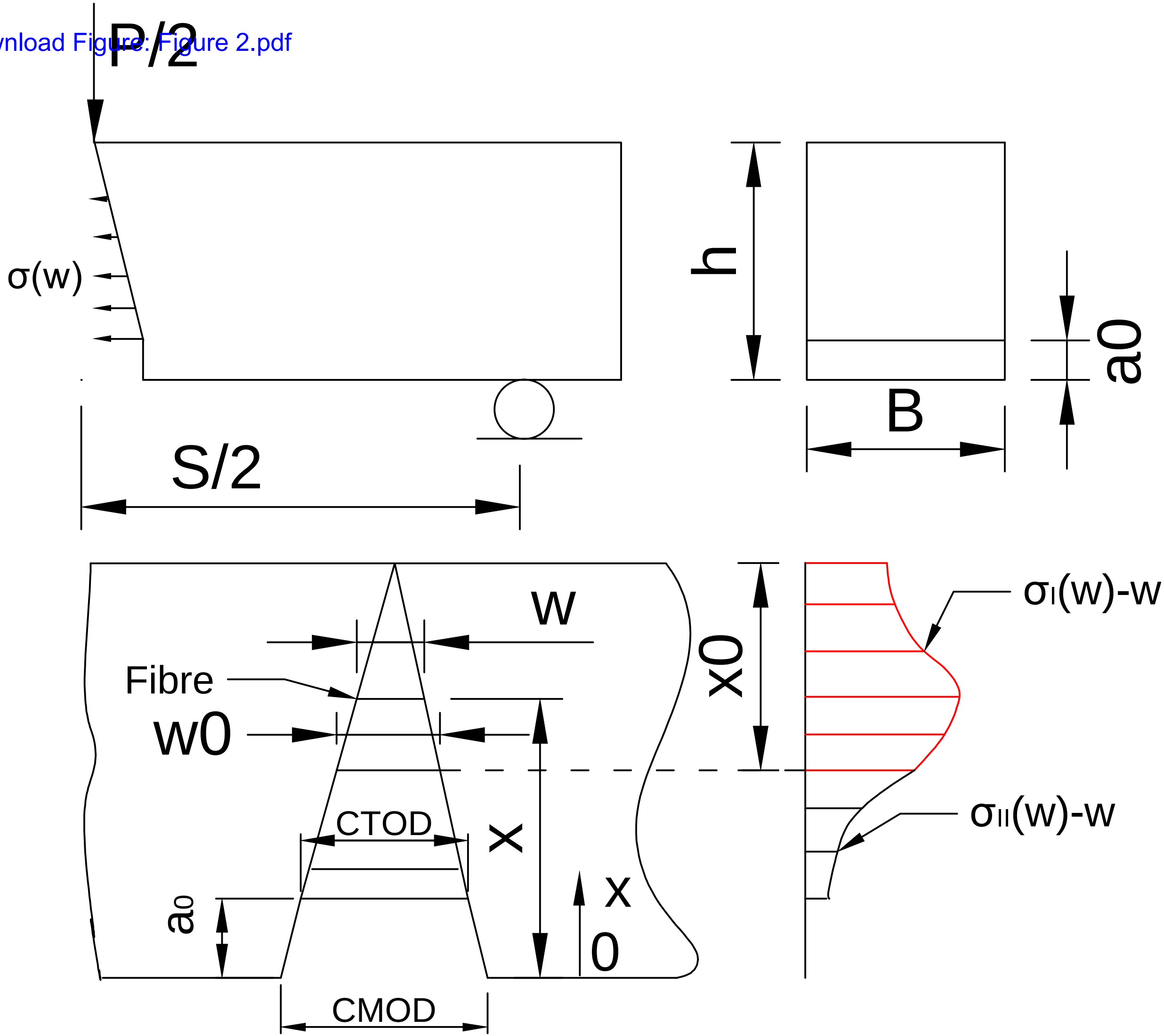
P/2
σ(w)
h
a0
B
S/2
w
Fibre
w0
x0
σI(w)-w
σII(w)-w
CTOD
x
x
0
a0
CMOD

Figure

Click here to download Figure: Figure 3.pdf

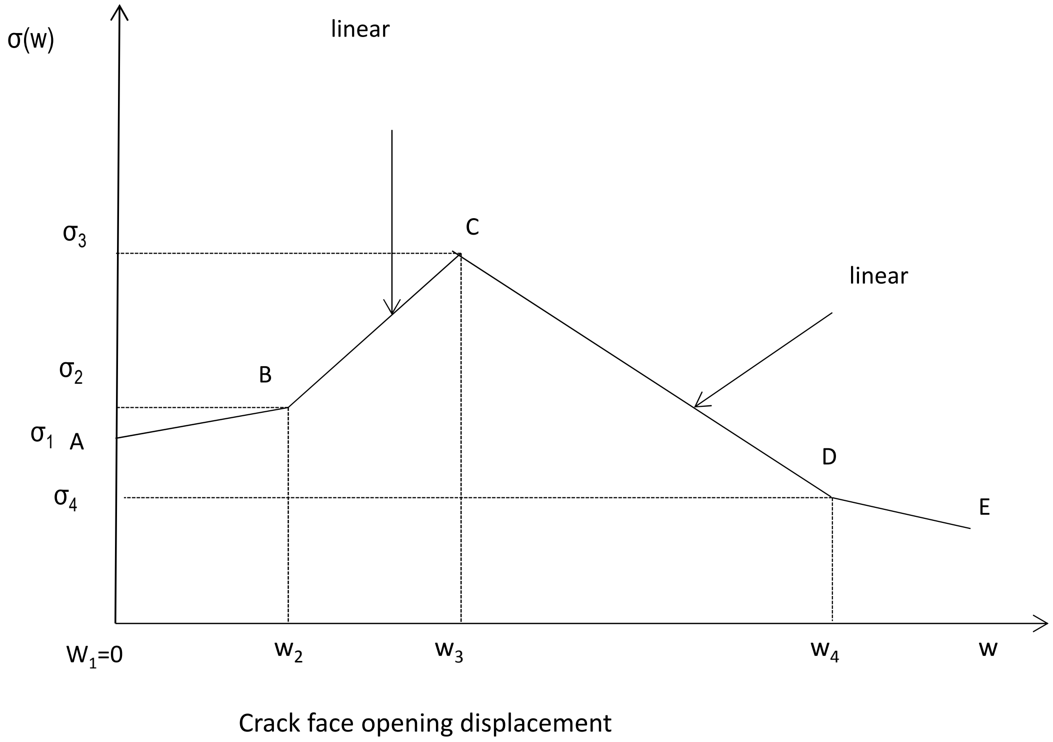

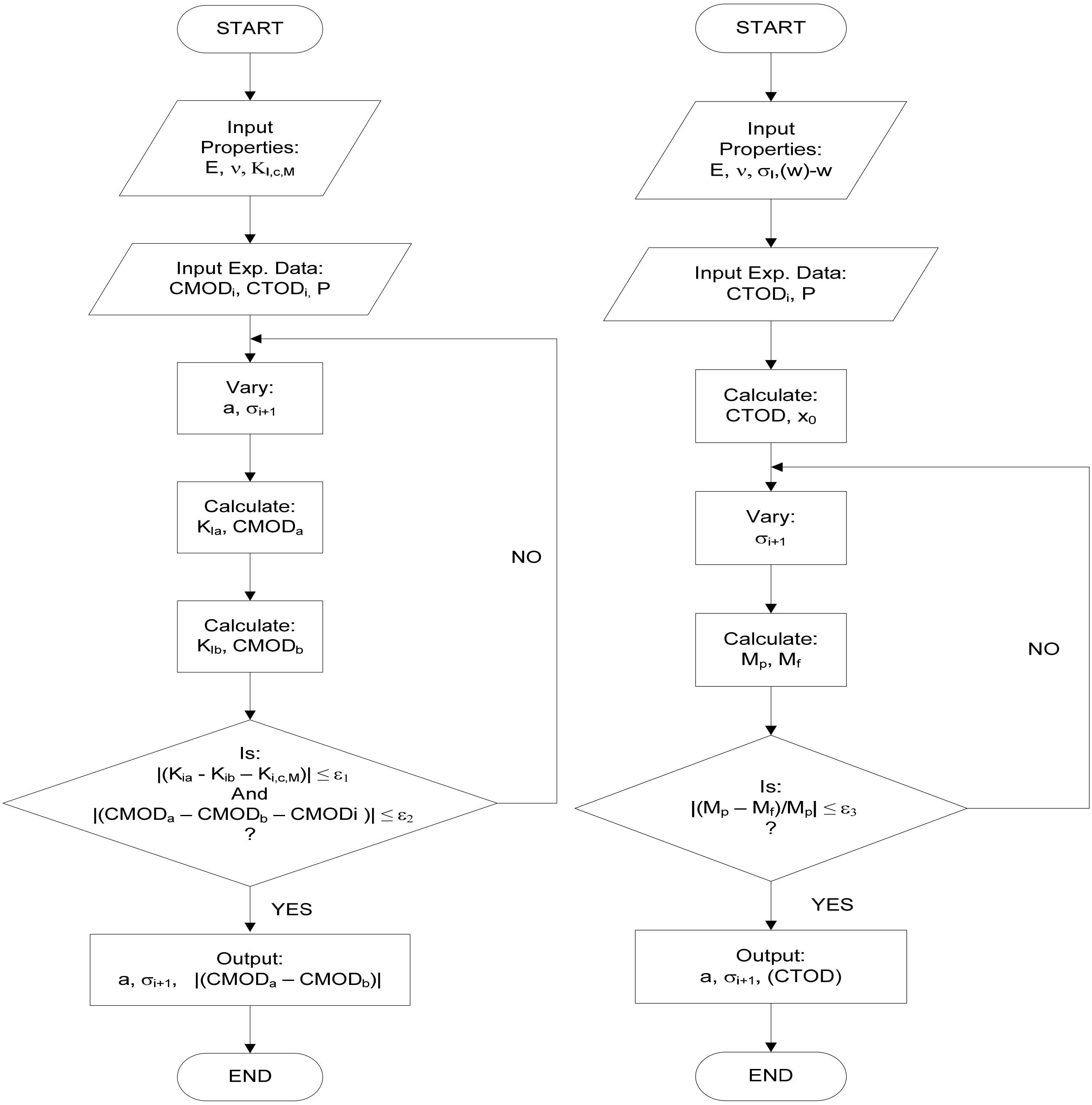
START
Input
Properties:
E, ν, K_{I,c,M}
Input Exp. Data:
CMOD_i, CTOD_i, P
Vary:
a, σ_{i+1}
Calculate:
K_{Ia}, CMOD_a
Calculate:
K_{Ib}, CMOD_b
NO
Is:
|(K_{ia} - K_{ib} – K_{i,c,M})| ≤ ε_1
And
|(CMOD_a – CMOD_b – CMODi)| ≤ ε_2
?
YES
Output:
a, σ_{i+1}, |(CMOD_a – CMOD_b)|
END
START
Input
Properties:
E, ν, σ_I,(w)-w
Input Exp. Data:
CTOD_i, P
Calculate:
CTOD, x_0
Vary:
σ_{i+1}
Calculate:
M_p, M_f
NO
Is:
|(M_p – M_f)/M_p| ≤ ε_3
?
YES
Output:
a, σ_{i+1}, (CTOD)
END

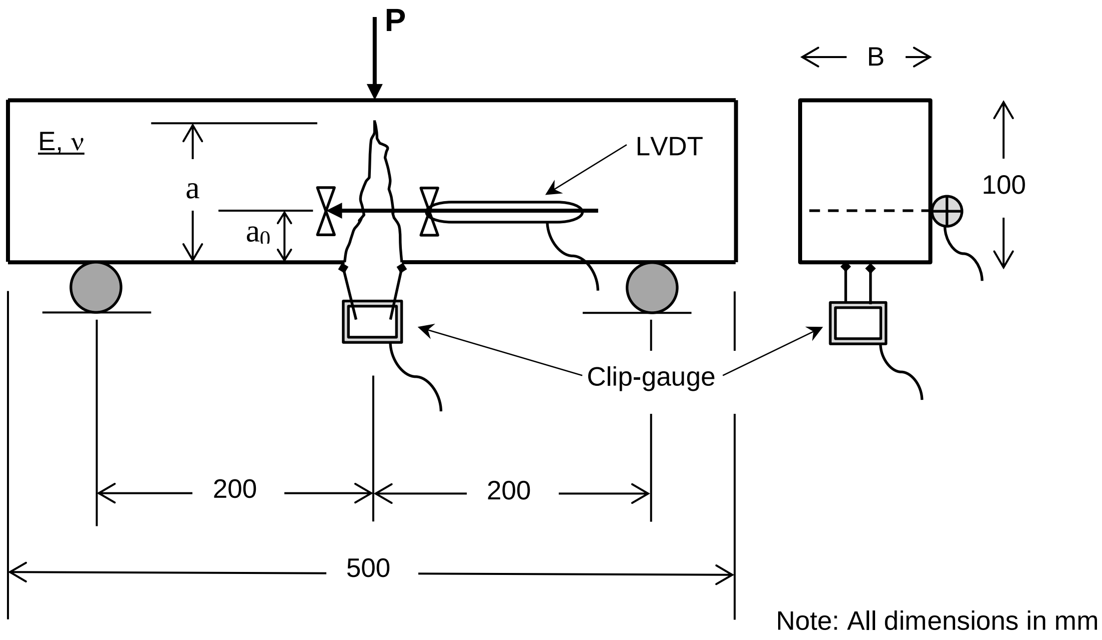
P
B
E, ν
a
a_0
LVDT
100
Clip-gauge
200
200
500
Note: All dimensions in mm

Figure
Click here to download Figure: Figure 5(b).pdf

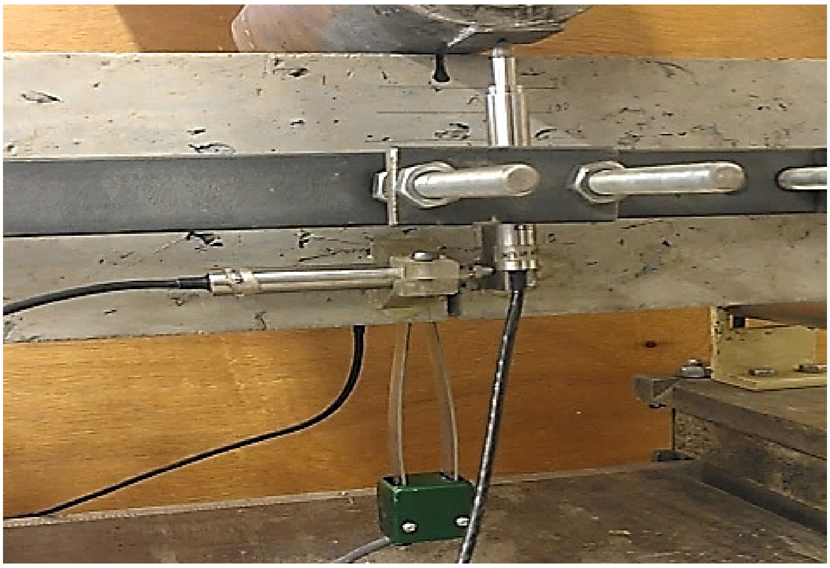

Figure

Click here to download Figure: Figure 6.pdf

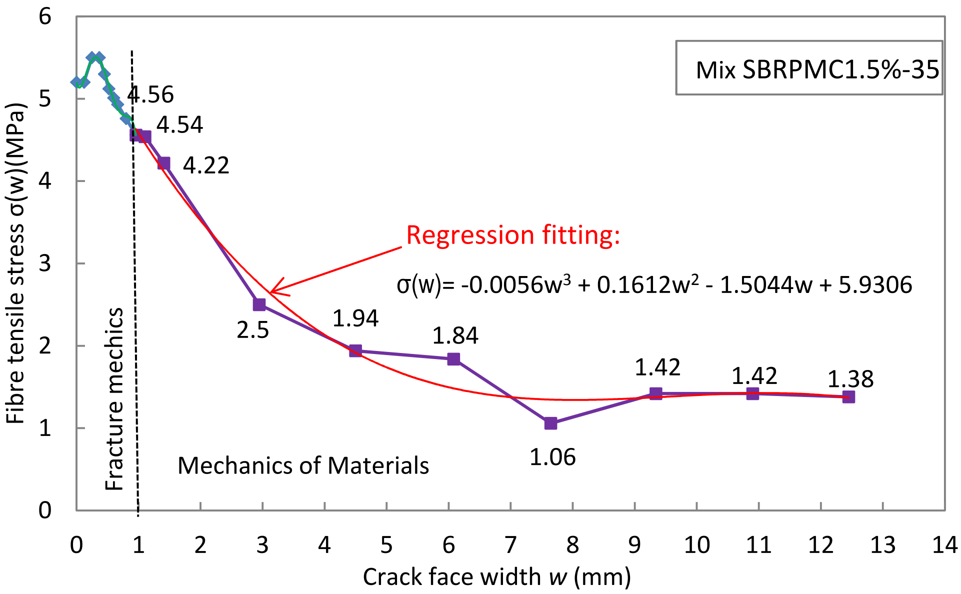

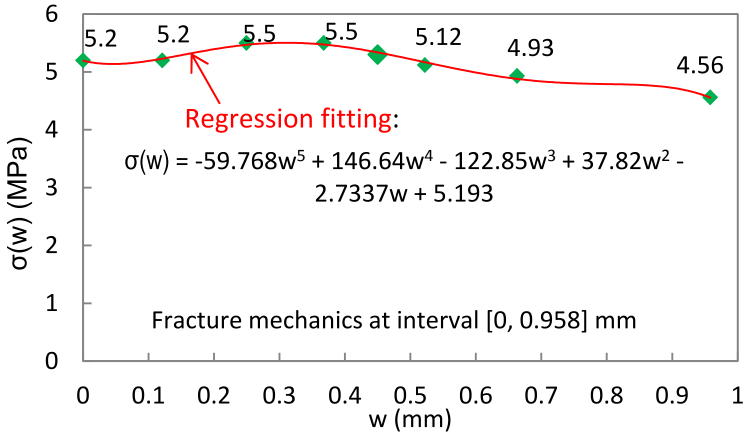
6
5
4
3
2
1
0
5.2
5.2
5.5
5.5
5.12
4.93
4.56
Regression fitting:
σ(w) = -59.768w⁵ + 146.64w⁴ - 122.85w³ + 37.82w² - 2.7337w + 5.193
σ(w) (MPa)
Fracture mechanics at interval [0, 0.958] mm
0 0.1 0.2 0.3 0.4 0.5 0.6 0.7 0.8 0.9 1
w (mm)

Figure

Click here to download Figure: Figure 8.pdf

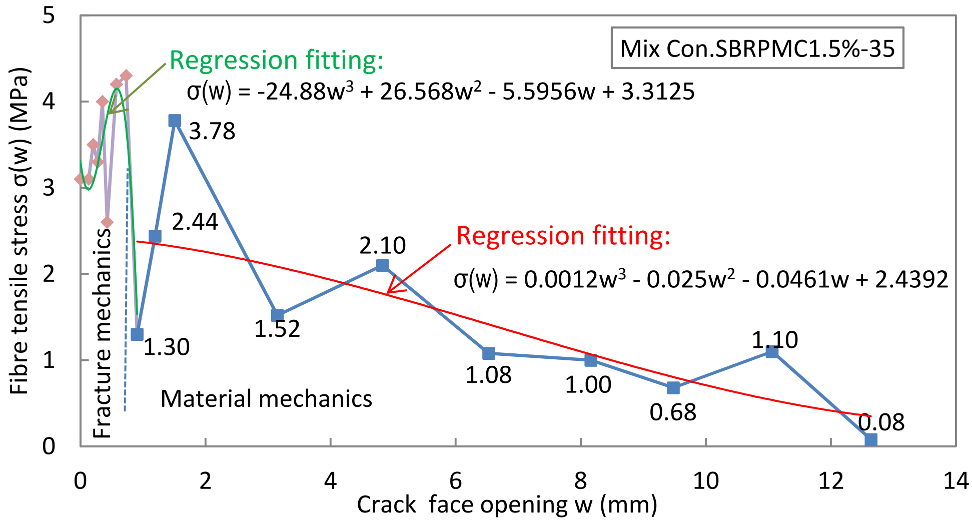

Figure
Click here to download Figure: Figure 9.pdf

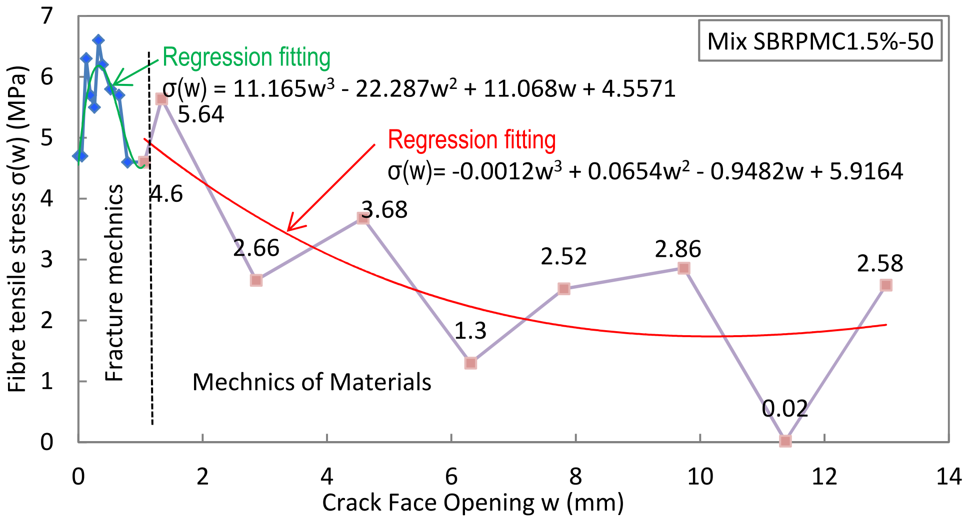

Figure
Click here to download Figure: Figure 10(a).pdf

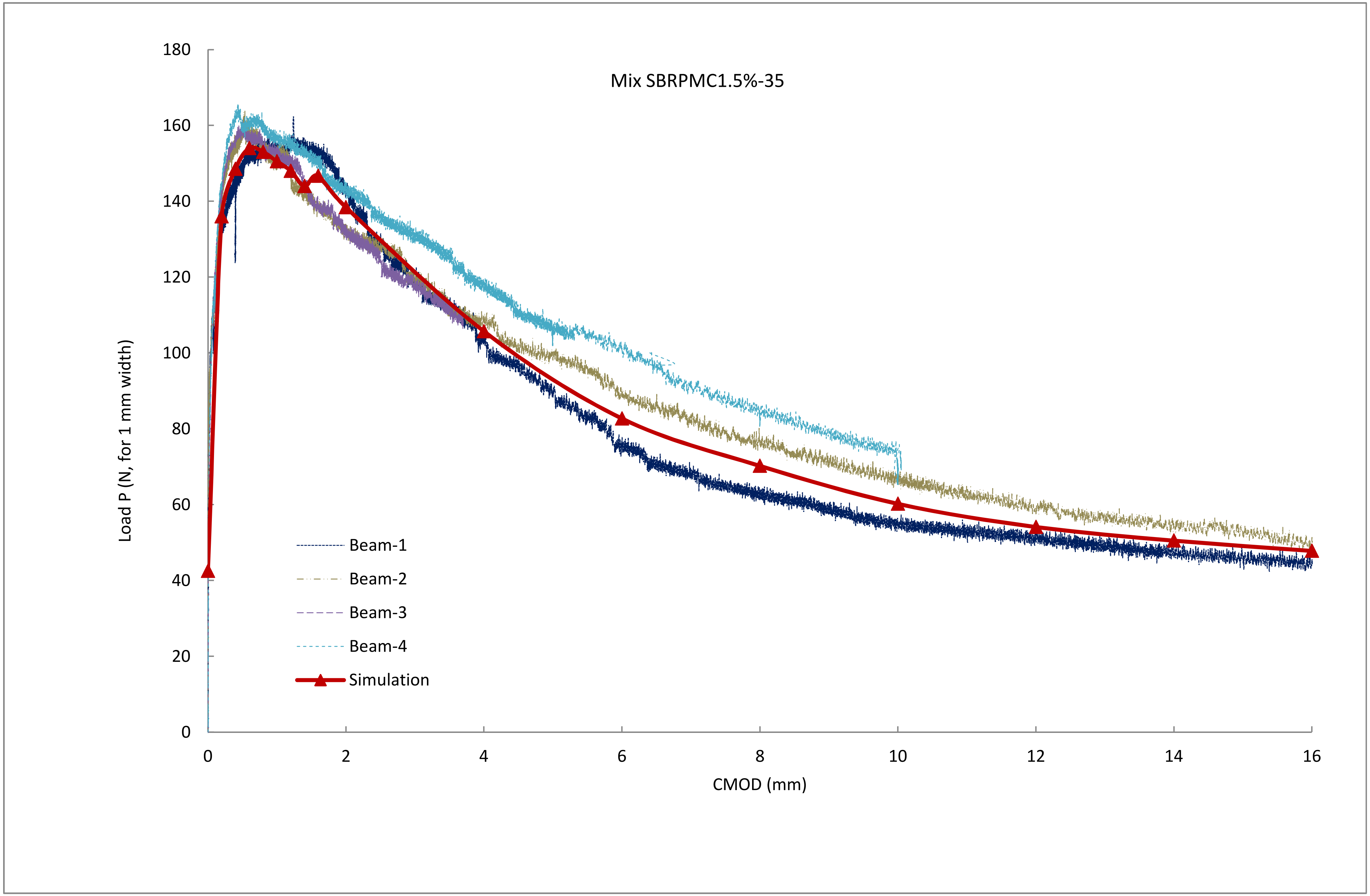

Figure
Click here to download Figure: Figure 10(b).pdf

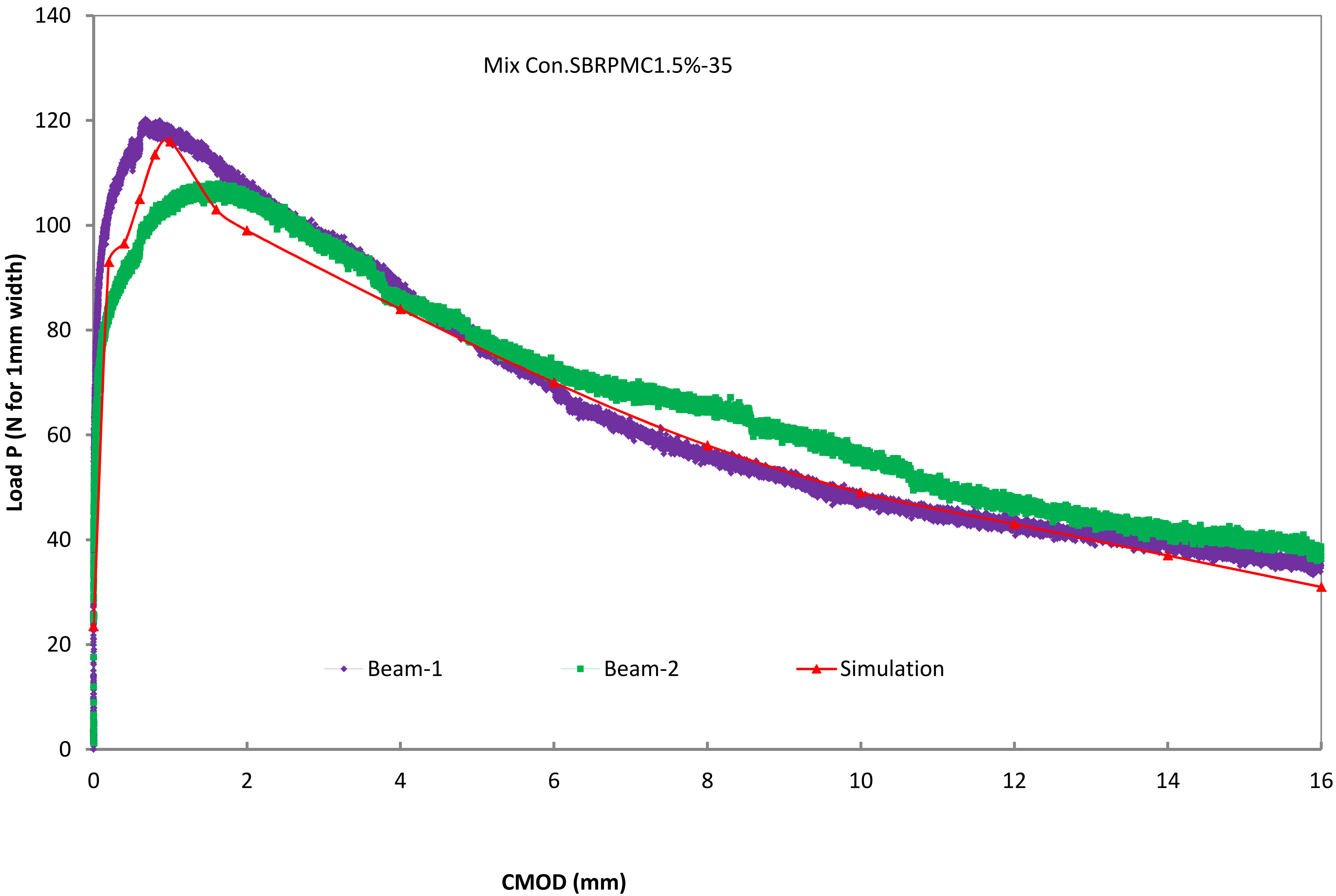

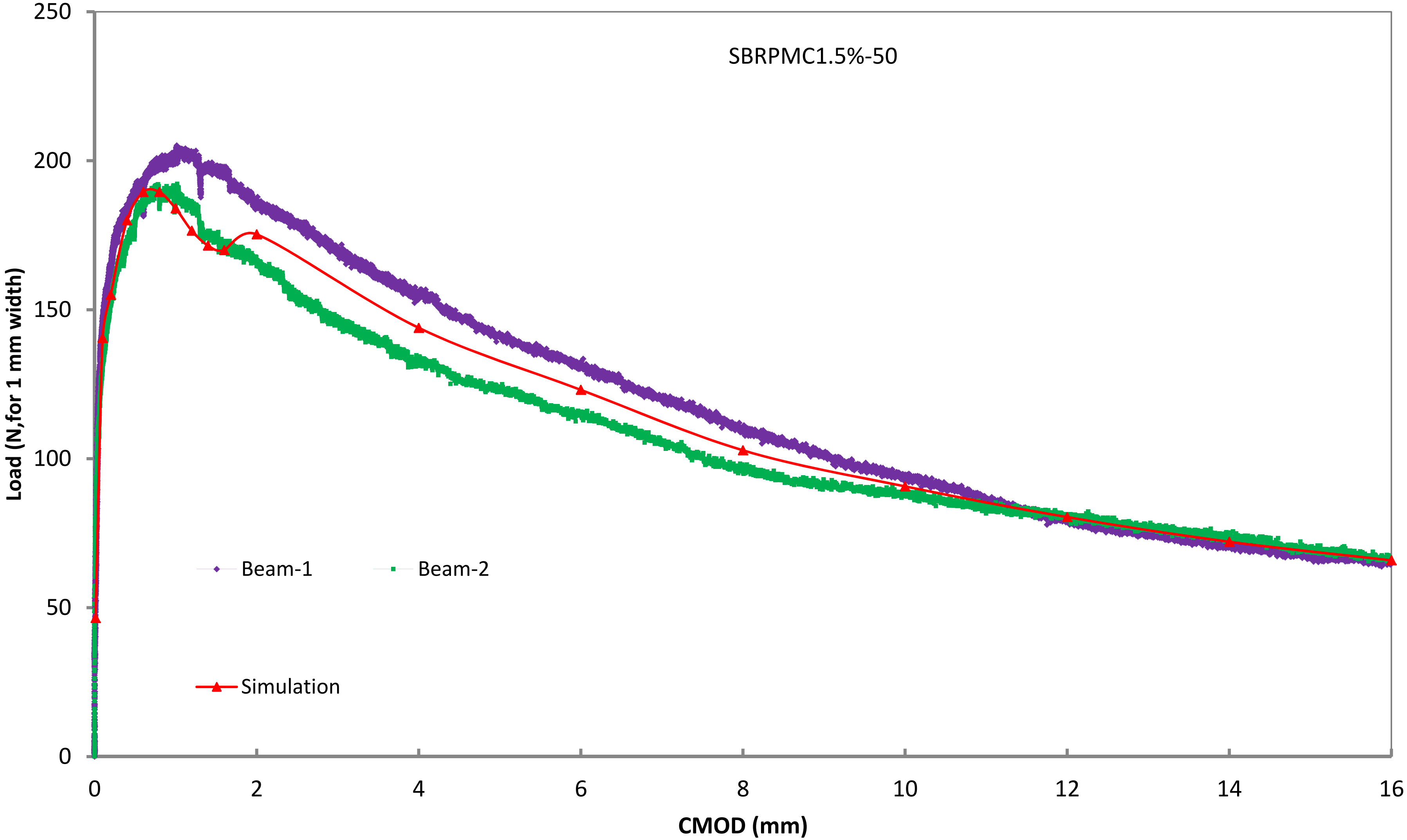
SBRPMC1.5%-50
Load (N,for 1 mm width)
CMOD (mm)
Beam-1
Beam-2
Simulation
0
50
100
150
200
250
0
2
4
6
8
10
12
14
16

Figure
Click here to download Figure: Figure 12.pdf